A SEMI-ANALYTICAL APPROACH FOR STRESS CONCENTRATION OF CANTILEVER BEAMS WITH HOLES UNDER BENDING

J.-T. Chen * **P.-Y. Chen** **

Department of Harbor and River Engineering
National Taiwan Ocean University
Keelung, Taiwan 20224, R.O.C.

ABSTRACT

In the paper, the degenerate kernels and Fourier series expansions are adopted in the null-field integral equation to solve bending problems of a circular beam with circular holes. The main gain of using degenerate kernels in integral equations is free of calculating the principal values for singular integrals. An adaptive observer system is addressed to fully employ the property of degenerate kernels for circular boundaries in the polar coordinate. After moving the null-field point to the boundary and matching the boundary conditions, a linear algebraic system is obtained without boundary discretization. The unknown coefficients in the algebraic system can be easily determined. The present method is treated as a "semi-analytical" solution since error only attributes to the truncation of Fourier series. Stress concentration is also our concern. Finally, several examples, including two holes and four holes, are given to demonstrate the validity of the proposed method. The results are compared with those of Naghdi and Bird and Steele. Also, the position where the maximum concentration factor occurs is examined. The present formulation can be extended to handle beam problems with arbitrary number and various positions of circular holes by using the developed general-purpose program.

Keywords : Null-field integral equation, Degenerate kernel, Fourier series, Circular holes, Cantilever beam, Stress concentration.

1. INTRODUCTION

The stress concentration around holes of a beam under bending or torsion plays an important role in promoting the design criteria for higher factors of safety. Many investigators [1,2,3] have studied the bending problems in different ways. Those problems have been visited in a few investigations based on the Saint-Venant theory [4,5]. For a simple case, an analytical solution may be available. Since the analytical solution for more than two holes may encounter difficulty, several numerical approaches have been employed, *e.g.* complex variable boundary element method (CVBEM) by Chou [6] and Ang and Kang [7]. The CVBEM was primarily introduced by Hromadka and Lai [8] for solving the Laplace problems in an infinite domain. In 1997, Chou extended the work of Hromadka to problems with the multiply-connected domain. Recently, Ang and Kang [7] developed a general formulation for solving the second-order elliptic partial differential equation for a multiply-connected region in a different version of CVBEM. The Cauchy integral formulae are offered to solve the boundary value problem. By introducing the CVBEM, Chou [1] and Ang and Kang [7] have revisited the anti-plane problems with two circular holes whose centers lie on the x axis investigated by Honein *et al.* [9]. Chen *et al.* [10] employed the null-field integral equation to solve the Laplace problem. In 1991, Naghdi [11] employed a special class of basic function, which is a Saint-Venant flexure function suitable for the problem of the bending of a circular cylinder with $4N$ (N = 1, 2, 3$\cdots$) circular holes in the axial direction. Bird and Steele [12] used a Fourier series procedure to revisit the antiplane problems in the Honein's paper [9]. Also, they revisited the bending problems which were solved by Naghdi [11]. According to the literature review, it is observed that exact solutions for boundary value problems are only limited for simple cases. Although Naghdi [11] has proposed a solution for bending problems with holes, it is limited for $4N$ (N = 1, 2, 3$\cdots$) holes. Therefore, proposing a systematic approach for solving BVP with various numbers of circular boundaries and arbitrary positions and radii is our goal in this paper. Following the success of anti-plane problems with circular holes [10], the null-field integral equation is utilized to solve the Saint-Venant bending problem of a beam with circular holes. The mathematical formulation is derived by using degenerate kernels for fundamental solutions and Fourier series for boundary densities in formulation. Then, it reduces to a linear algebraic equation by collocation approach. After determining the unknown coefficients,

* Life-Time Distinguished Professor ** Master student

series solution for the bending function is obtained. Both the location of maximum stress concentration factor (SCF) and the boundary layer effect are addressed. Numerical examples are given to show the validity and efficiency of our approach.

2. PROBLEM STATEMENT

Consider a beam with a circular section weakened by four circular holes placed on a concentric ring of radius a as shown in Fig. 1. The radii of outer circle and inner holes are R and b, respectively. The beam is subject to a shear force Q at the free end, and the boundary conditions of outer circle and inner holes are traction free. Following the theory of Saint-Venant bending, we assume the stress to be

$$\sigma_{xx} = \sigma_{yy} = \sigma_{xy} \equiv 0\,,\ \sigma_{zz} = -\frac{Q}{I_y} x(l-z)\,, \tag{1}$$

where I_y is the moment of inertia of cross section for the y-axis. The other two stress components are assumed as

$$\sigma_{zx} = \alpha\mu\left(\frac{\partial\varphi}{\partial x} + y\right) - \frac{Q}{2(1+\nu)I_y}\left[\frac{\partial\psi}{\partial x} + \frac{1}{2}\nu x^2 + \left(1-\frac{1}{2}\nu\right)y^2\right], \tag{2}$$

$$\sigma_{zy} = \alpha\mu\left(\frac{\partial\varphi}{\partial y} + x\right) - \frac{Q}{2(1+\nu)I_y}\left[\frac{\partial\psi}{\partial y} + (2+\nu)xy\right], \tag{3}$$

where $\varphi(x, y)$ and $\psi(x, y)$ are the warping function and bending function of the beam, respectively, α is the angle of twist per unit length, and μ is the shear modulus. Since the $\varphi(x, y)$ and $\psi(x, y)$ in the Saint-Venant bending problem satisfy the two Laplace equations subject to the Neumann boundary condition, we have:

$$\nabla^2\varphi(x, y) = \frac{\partial^2\varphi}{\partial x^2} + \frac{\partial^2\varphi}{\partial y^2} = 0 \ \text{ in } \ D\,, \tag{4}$$

$$\frac{\partial\varphi}{\partial n} = y\cos(n, x) - x\cos(n, y) \quad x, y \in B_i\,, \tag{5}$$

and

$$\nabla^2\psi(x, y) = \frac{\partial^2\psi}{\partial x^2} + \frac{\partial^2\psi}{\partial y^2} = 0 \ \text{ in } \ D\,, \tag{6}$$

$$\frac{\partial\psi}{\partial n} = -\left[\frac{1}{2}\nu x^2 + \left(1-\frac{1}{2}\nu\right)y^2\right]\cos(n, x) - (2+\nu)xy\cos(n, y) \quad x, y \in B_k \tag{7}$$

where D is the domain of interest, n is the outward normal vector of each boundary, and B_k is the kth circular boundary. In Fig. 1, we define the position vector of the boundary point of the kth circular boundary as

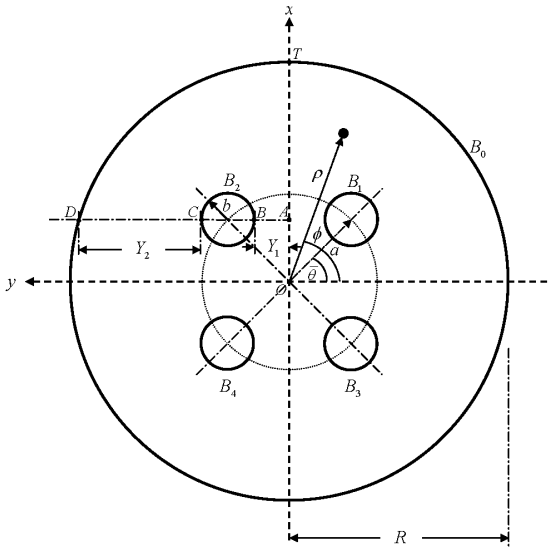

Fig. 1 Cross-section of cantilever beam of symmetrical holes

$$x = R_k \sin\theta_k + x_k\,,\ k = 0, 1, 2, 3, 4, \quad 0 < \theta_k < 2\pi \tag{8}$$

$$y = -R_k \cos\theta_k + y_k\,,\quad k = 0, 1, 2, 3, 4, \quad 0 < \theta_k < 2\pi \tag{9}$$

where

$$R_0 = R \quad \text{and} \quad R_k = b, \quad k = 1, 2, 3, 4 \tag{10}$$

and θ_k is the polar angle with respect to the origin of the kth hole, (x_k, y_k) are the coordinate for the center of the kth eccentric circle, and the eccentricity is zero for the outer circle. By substituting Eqs. (8) and (9) into Eq. (7) , the Neumann boundary condition can be specified.

For the simple case of bending only, we can assume constant $\alpha\mu$ and $\varphi(x, y)$ to be zero. Following the definition of stress concentration by Naghdi [11], we have

$$Sc = \frac{\sigma_{zx} A}{Q} \tag{11}$$

where A is the area of the cross-section. The shear stress σ_{zx} in Eq. (11) is obtained from Eq. (2). Thus, the problem of bending is reduced to find the bending function $\psi(x, y)$ which satisfies the Laplace equation of Eq. (6) and the Neumann boundary condition of Eq. (7) on each boundary.

3. DUAL BOUNDARY INTEGRAL EQUATIONS AND DUAL NULL-FIELD INTEGRAL EQUATIONS

Employing the Fourier series expansions to approximate the potential u and its normal derivative t on the circular boundary, we have

$$u(\mathrm{s}_k) = a_0^k + \sum_{n=1}^{\infty}(a_n^k \cos n\theta_k + b_n^k \sin n\theta_k)\,, \quad \mathrm{s}_k \in B_k\,,\ k = 0, 1, \cdots, N\,, \tag{12}$$

$$t(\mathrm{s}_k) = p_0^k + \sum_{n=1}^{\infty} (p_n^k \cos n\theta_k + q_n^k \sin n\theta_k) , \quad \mathrm{s}_k \in B_k , \quad k = 0, 1, \cdots, N , \tag{13}$$

where $t(s_k) = \partial u(s_k)/\partial n_s$ in which n_s denotes the outward normal vector at the source point s, a_n^k, b_n^k, p_n^k and q_n^k (n = 0, 1, 2, $\cdots$) are the Fourier coefficients and θ_k is the polar angle for the kth circular boundary. The integral equation for the domain point can be derived from the third Green's identity [13], we have

$$2\pi u(\mathrm{x}) = \int_B T(\mathrm{s}, \mathrm{x})\, u(\mathrm{s})\, dB(\mathrm{s}) - \int_B U(\mathrm{s}, \mathrm{x})\, t(\mathrm{s})\, dB(\mathrm{s}) , \quad \mathrm{x} \in D , \tag{14}$$

$$2\pi t(\mathrm{x}) = \int_B M(\mathrm{s}, \mathrm{x})\, u(\mathrm{s})\, dB(\mathrm{s}) - \int_B L(\mathrm{s}, \mathrm{x})\, t(\mathrm{s})\, dB(\mathrm{s}), \quad \mathrm{x} \in D , \tag{15}$$

where s and x are the source and field points, respectively, B is the boundary, D is the domain of interest, and the kernel function $U(\mathrm{s}, \mathrm{x}) = \ln r$, ($r \equiv |\mathrm{x} - \mathrm{s}|$), is the fundamental solution which satisfies

$$\nabla^2 U(\mathrm{s}, \mathrm{x}) = 2\pi\delta(\mathrm{x} - \mathrm{s}) , \tag{16}$$

where $\delta(\mathrm{x} - \mathrm{s})$ denotes the Dirac-delta function. The other kernel functions, $T(\mathrm{s}, \mathrm{x})$, $L(\mathrm{s}, \mathrm{x})$ and $M(\mathrm{s}, \mathrm{x})$, are defined by

$$T(\mathrm{s}, \mathrm{x}) \equiv \frac{\partial U(\mathrm{s}, \mathrm{x})}{\partial \mathrm{n}_\mathrm{s}} , \quad L(\mathrm{s}, \mathrm{x}) \equiv \frac{\partial U(\mathrm{s}, \mathrm{x})}{\partial \mathrm{n}_\mathrm{x}} , \quad M(\mathrm{s}, \mathrm{x}) \equiv \frac{\partial^2 U(\mathrm{s}, \mathrm{x})}{\partial \mathrm{n}_\mathrm{s} \partial \mathrm{n}_\mathrm{x}} , \tag{17}$$

By collocating x outside the domain ($\mathrm{x} \in D^c$), we obtain the dual null-field integral equations as shown below

$$0 = \int_B T(\mathrm{s}, \mathrm{x})\, u(\mathrm{s})\, dB(\mathrm{s}) - \int_B U(\mathrm{s}, \mathrm{x})\, t(\mathrm{s})\, dB(\mathrm{s}) , \quad \mathrm{x} \in D^c , \tag{18}$$

$$0 = \int_B M(\mathrm{s}, \mathrm{x})\, u(\mathrm{s})\, dB(\mathrm{s}) - \int_B L(\mathrm{s}, \mathrm{x})\, t(\mathrm{s})\, dB(\mathrm{s}) , \quad \mathrm{x} \in D^c , \tag{19}$$

where D^c is the complementary domain. Based on the separable property, the kernel function $U(\mathrm{s}, \mathrm{x})$ is expanded into the degenerate form by separating the source point ($\mathrm{s} = (R, \theta)$) and field point ($\mathrm{x} = (\rho, \phi)$) in the polar coordinate [14]:

$$U(\mathrm{s}, \mathrm{x}) = \begin{cases} U^i(R, \theta; \rho, \phi) = \ln R - \sum_{m=1}^{\infty} \frac{1}{m} \left(\frac{\rho}{R}\right)^m \cos m(\theta - \phi), & R \geq \rho \\ U^e(R, \theta; \rho, \phi) = \ln \rho - \sum_{m=1}^{\infty} \frac{1}{m} \left(\frac{R}{\rho}\right)^m \cos m(\theta - \phi), & \rho > R \end{cases} , \tag{20}$$

where the superscripts "i" and "e" denote the interior ($R > \rho$) and exterior ($\rho > R$) cases, respectively. It is found that the leading term and numerator term contain the larger argument to ensure log singularity and series convergence, respetively. After taking the normal derivative ($\partial/\partial R$) with respect to Eq. (19), the $T(\mathrm{s}, \mathrm{x})$ kernel function yields

$$T(\mathrm{s}, \mathrm{x}) = \begin{cases} T^i(R, \theta; \rho, \phi) = \frac{1}{R} + \sum_{m=1}^{\infty} \left(\frac{\rho^m}{R^{m+1}}\right) \cos m(\theta - \phi) , & R > \rho \\ T^e(R, \theta; \rho, \phi) = -\sum_{m=1}^{\infty} \left(\frac{R^{m-1}}{\rho^m}\right) \cos m(\theta - \phi) , & \rho > R \end{cases} , \tag{21}$$

and the higher-order kernel functions, $L(\mathrm{s}, \mathrm{x})$ and $M(\mathrm{s}, \mathrm{x})$, are shown below:

$$L(\mathrm{s}, \mathrm{x}) = \begin{cases} L^i(R, \theta; \rho, \phi) = -\sum_{m=1}^{\infty} \left(\frac{\rho^{m-1}}{R^m}\right) \cos m(\theta - \phi) , & R > \rho \\ L^e(R, \theta; \rho, \phi) = \frac{1}{\rho} + \sum_{m=1}^{\infty} \left(\frac{R^m}{\rho^{m+1}}\right) \cos m(\theta - \phi) , & \rho > R \end{cases} , \tag{22}$$

$$M(\mathrm{s}, \mathrm{x}) = \begin{cases} M^i(R, \theta; \rho, \phi) = \sum_{m=1}^{\infty} \left(\frac{m\rho^{m-1}}{R^{m+1}}\right) \cos m(\theta - \phi) , & R \geq \rho \\ M^e(R, \theta; \rho, \phi) = \sum_{m=1}^{\infty} \left(\frac{mR^{m-1}}{\rho^{m+1}}\right) \cos m(\theta - \phi) , & \rho > R \end{cases} . \tag{23}$$

Since the potentials resulted from $T(\mathrm{s}, \mathrm{x})$ and $L(\mathrm{s}, \mathrm{x})$ are discontinuous cross the boundary, the potentials of $T(\mathrm{s}, \mathrm{x})$ and $L(\mathrm{s}, \mathrm{x})$ for $R \to \rho^+$ and $R \to \rho^-$ are different. This is the reason why $R = \rho$ is not included in the expression for the degenerate kernels of $T(\mathrm{s}, \mathrm{x})$ and $L(\mathrm{s}, \mathrm{x})$ in Eqs. (21) and (22). The analytical evaluation of the integrals for each element in the influence matrix is listed in the Appendix and they are all non-singular. Besides, the limiting case to the boundary is also addressed. The continuous and jump behavior across the boundary is also described. For example, the jump behavior is captured by

$$\int_0^{2\pi} \left(T^i(\mathrm{s}, \mathrm{x}) - T^e(\mathrm{s}, \mathrm{x})\right) \cos(m\theta)\, Rd\theta = 2\pi \cos(m\theta) , \quad x \in B \tag{24}$$

$$\int_0^{2\pi} \left(T^i(\mathrm{s}, \mathrm{x}) - T^e(\mathrm{s}, \mathrm{x})\right) \sin(m\theta) Rd\theta = 2\pi \sin(m\theta) , \quad x \in B \tag{25}$$

where the above equation is equivalent to the Wronskian of two bases for 1-D case.

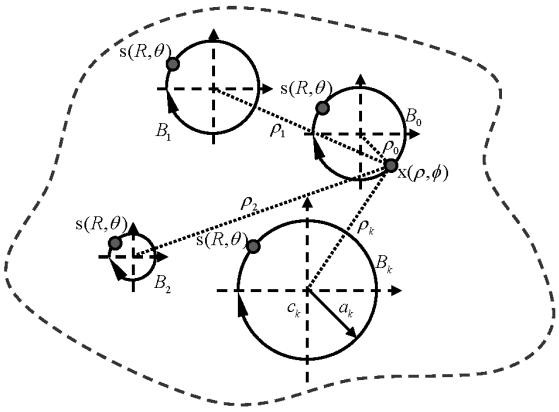

Fig. 2(a) Sketch of the null-field integral equation in conjunction with the adaptive observer system

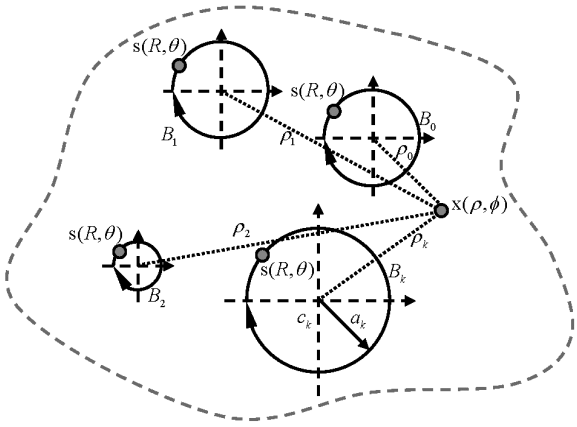

Fig. 2(b) Sketch of the boundary integral equation for domain point in conjunction with the adaptive observer system

4. ADAPTIVE OBSERVER SYSTEM

After moving the null-field point of Eq. (18) to the boundary, the boundary integrals through all the circular contours are required to be calculated. Since the boundary integral equations are frame indifferent (rule of objectivity) due to the energy or work form, the observer system is adaptively to locate the origin at the center of circle under integration. Adaptive observer system is chosen to fully employ the property of degenerate kernels. Figures 2(a) and 2(b) show the boundary integration for the circular boundaries in the adaptive observer system. The origin of the observer system is located on the center of the corresponding circle under integration to entirely utilize the geometry of circular boundary for the expansion of degenerate kernels and boundary densities.

5. VECTOR DECOMPOSTION TECHNIQUE OF THE POTENTIAL GRADIENT FOR THE STRESS CALCULATION IN THE HYPER SINGULAR FORMULATION

The hypersingular integral equation in Eq. (2) ~ (15) is defined as the normal derivative of potential for the domain points (x), special treatment is considered here. Not only for calculating the stress but also for degenerate scales [15~17], potential gradient on the boundary using hypersingular formulation is required to calculate. Consider the nonconcentric case as shown in Fig. 3, the true normal direction ($\bar{1}$) with respect to the collocation point x on the B_i boundary can be superimposed by using the radial direction ($\bar{3}$) and angular direction ($\bar{4}$) on the B_j boundary. According to the concept of decomposition technique, the degenerate kernels for the higher-order singular equation as Eqs. (22) and (23) are changed as:

$$L(\mathrm{s},\mathrm{x}) = \begin{cases} L^{i}(R,\theta;\rho,\phi) = -\sum_{m=1}^{\infty}\left(\frac{\rho^{m-1}}{R^{m}}\right)\cos m(\theta-\phi)\cos(\zeta-\xi) \\ \qquad -\sum_{m=1}^{\infty}\left(\frac{\rho^{m-1}}{R^{m}}\right)\sin m(\theta-\phi)\cos\left(\frac{\pi}{2}-\zeta+\xi\right), \quad R>\rho \\ L^{e}(R,\theta;\rho,\phi) = \frac{1}{\rho}+\sum_{m=1}^{\infty}\left(\frac{R^{m}}{\rho^{m+1}}\right)\cos m(\theta-\phi)\cos(\zeta-\xi) \\ \qquad -\sum_{m=1}^{\infty}\left(\frac{R^{m}}{\rho^{m+1}}\right)\sin m(\theta-\phi)\cos\left(\frac{\pi}{2}-\zeta+\xi\right), \quad \rho>R \end{cases} \tag{26}$$

$$M(\mathrm{s},\mathrm{x}) = \begin{cases} M^{i}(R,\theta;\rho,\phi) = \sum_{m=1}^{\infty}\left(\frac{m\rho^{m-1}}{R^{m+1}}\right)\cos m(\theta-\phi)\cos(\zeta-\xi) \\ \qquad -\sum_{m=1}^{\infty}\left(\frac{m\rho^{m-1}}{R^{m+1}}\right)\sin m(\theta-\phi)\cos\left(\frac{\pi}{2}-\zeta+\xi\right), \quad R\geq\rho \\ M^{e}(R,\theta;\rho,\phi) = \sum_{m=1}^{\infty}\left(\frac{mR^{m-1}}{\rho^{m+1}}\right)\cos m(\theta-\phi)\cos(\zeta-\xi) \\ \qquad -\sum_{m=1}^{\infty}\left(\frac{mR^{m-1}}{\rho^{m+1}}\right)\sin m(\theta-\phi)\cos\left(\frac{\pi}{2}-\zeta+\xi\right), \quad \rho>R \end{cases} \tag{27}$$

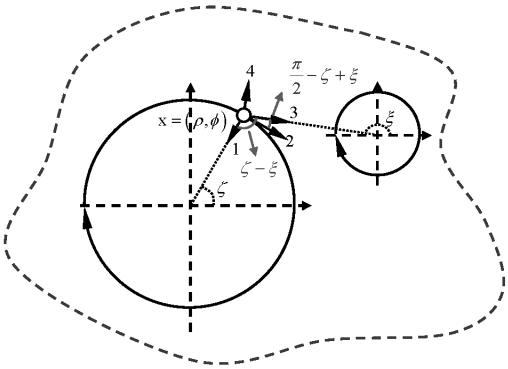

1: True normal direction
2: True tangential direction
3: Normal direction
4: Tangential direction

Fig. 3 Vector decomposition for the potential gradient for stress calculation in the hypersingular equation

where ζ and ξ are shown in Fig. 3. For the concentric case, the circles with respect to the same origin of observer, the potential gradient is derived free of special treatment since $\zeta = \xi$.

6. LINEAR ALGEBRAIC SYSTEM

We need to collocate $2M + 1$ null-field point on the boundary to calculate $2M + 1$ unknown Fourier coefficients. By moving the null-field point x_k on the kth circular boundary in the sense of limit for Eq. (18) in Fig. 2 (a), we have

$$0 = \sum_{k=0}^{N} \int_{B_k} T(\mathrm{s}_k, \mathrm{x}_j)\, u(\mathrm{s}_k)\, dB_k(\mathrm{s}) - \sum_{k=0}^{N} \int_{B_k} U(\mathrm{s}_k, \mathrm{x}_j)\, t(\mathrm{s}_k)\, dB_k(\mathrm{s}) \ , \ \mathrm{x} \in D^c , \tag{28}$$

where N is the number of inner circular holes. By moving the null-field point on the boundary, a linear algebraic system is obtained

$$[\mathbf{U}]\{\mathbf{t}\} = [\mathbf{T}]\{\mathbf{u}\} , \tag{29}$$

where $[\mathbf{U}]$ and $[\mathbf{T}]$ are the influence matrices with a dimension of $(N + 1) \times (2M + 1)$ by $(N + 1) \times (2M + 1)$, $\{\mathbf{u}\}$ and $\{\mathbf{t}\}$ denote the column vectors of Fourier coefficients with a dimension of $(N + 1) \times (2M + 1)$ by one in which $[\mathbf{U}]$, $[\mathbf{T}]$, $\{\mathbf{u}\}$ and $\{\mathbf{t}\}$ can be defined as follows:

$$[\mathbf{U}] = \begin{bmatrix} \mathbf{U}_{00} & \mathbf{U}_{01} & \cdots & \mathbf{U}_{0N} \\ \mathbf{U}_{10} & \mathbf{U}_{11} & \cdots & \mathbf{U}_{1N} \\ \vdots & \vdots & \ddots & \vdots \\ \mathbf{U}_{N0} & \mathbf{U}_{N1} & \cdots & \mathbf{U}_{NN} \end{bmatrix}, \quad [\mathbf{T}] = \begin{bmatrix} \mathbf{T}_{00} & \mathbf{T}_{01} & \cdots & \mathbf{T}_{0N} \\ \mathbf{T}_{10} & \mathbf{T}_{11} & \cdots & \mathbf{T}_{1N} \\ \vdots & \vdots & \ddots & \vdots \\ \mathbf{T}_{N0} & \mathbf{T}_{N1} & \cdots & \mathbf{T}_{NN} \end{bmatrix}, \tag{30}$$

$$\{\mathbf{u}\} = \begin{Bmatrix} \mathbf{u}_0 \\ \mathbf{u}_1 \\ \mathbf{u}_2 \\ \vdots \\ \mathbf{u}_N \end{Bmatrix}, \quad \{\mathbf{t}\} = \begin{Bmatrix} \mathbf{t}_0 \\ \mathbf{t}_1 \\ \mathbf{t}_2 \\ \vdots \\ \mathbf{t}_N \end{Bmatrix}, \tag{31}$$

where the vectors $\{\mathbf{u}_k\}$ and $\{\mathbf{t}_k\}$ are in the form of $\{a_0^k \ \ a_1^k \ \ b_1^k \ \cdots \ a_M^k \ \ b_M^k\}^T$ and $\{p_0^k \ \ p_1^k \ \ q_1^k \ \cdots \ p_M^k \ \ q_M^k\}^T$, respectively; the first subscript "j" (j = 0, 1, 2,⋯, N) in $[\mathrm{U}_{jk}]$ and $[\mathrm{T}_{jk}]$ denotes the index of the *jth* circle where the collocation point is located and the second subscript "k" (k = 0, 1, 2,⋯, N) denotes the index of the *kth* circle where the boundary data $\{\mathbf{u}_k\}$ or $\{\mathbf{t}_k\}$ are specified, M indicates the truncated terms of Fourier series. By rearranging the known and unknown sets, the unknown Fourier coefficients are determined. Equation (18) can be calculated by employing the orthogonal property of Fourier bases in the real computation. Only the finite M terms are used in the summation of Eqs. (12) and (13). After obtaining the unknown Fourier coefficients, the boundary stress and interior potential can be easily calculated. A flowchart is shown in Fig. 4.

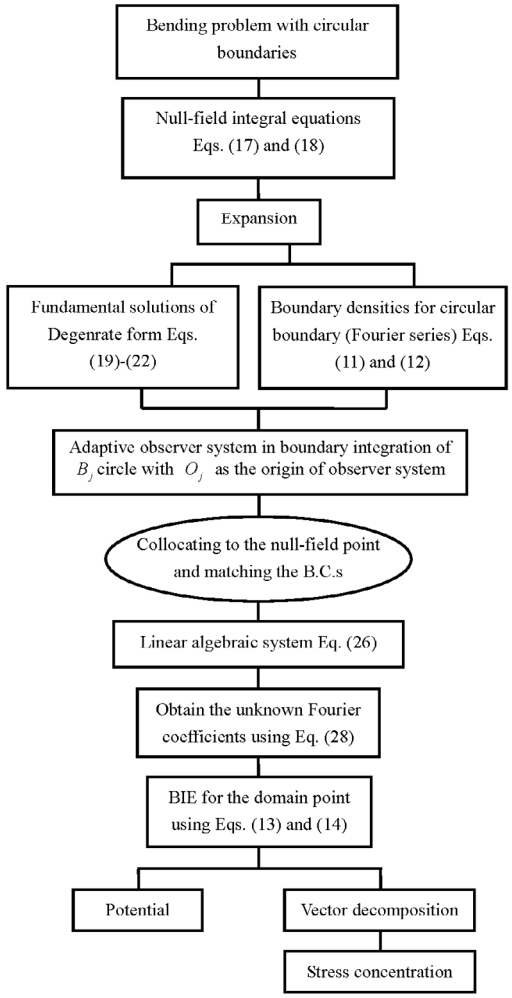

Fig. 4 Flowchart of the present method

7. ILLUSTRATIVE EXAMPLES AND DISCUSSIONS

Case 1. *Four circular holes* [11,12,18]

In order to check the validity of the present formulation, the Naghdi's problems for beam problems with four holes symmetrically located with respect to the x and y axis were revisited. All the numerical results were obtained by using ten terms of Fourier series (M = 10). We set the value of Poisson's ratio v = 0.3 and R = 1. In Figures 5 (a), (b), (d) and (e), the values of the stress concentration Sc along AB and CD (as Fig. 1) are plotted versus the position $\overline{Y}_1 = 17Y_1/AB$, and $\overline{Y}_2 = 17Y_2/CD$, respectively. Figures 5 (c) and (f) show the stress concentration Sc along OT, and the $\xi_1 = 18 \times OT$ for the case of a = 0.5, $\overline{\theta} = \pi/4$ and b = 0.1. Our numerical results are well compared with those of Naghdi's data [11]. In order to find the stress concentration on the holes, we plot the stress around the hole where these numerical results indicate that the Sc reaches maximum near the point B as shown in Fig. 6. Figures 5 (a) and (b) shows that the maximum value of Sc occurs at B and C respectively, where are on the boundaries of inner holes. For the Sc distribution along OT, the maximum value of Sc occurs at the position near the center of the two above holes. Good agreement is made after comparing with the Naghdi's results. In the literature, Naghdi [11] and Bird and Steele [12] also calculated the stress concentration factor at the point B for b = 0.12 and various values of a, Bird and Steele [12] stated that the deviation by Naghdi's data is 1!. The grounds for this discrepancy were not identified in their paper. Our numerical results are more agreeable to the Naghdi's data [11] as shown in Figs. 7 and 8, where Fig. 8 was not provided by Bird and Steele [12]. In order to verify the free boundary-layer effect at the present formulation, Fig. 9 shows the Sc distribution near the boundary. According to the convergence test in Fig. 10, only eight terms (M = 8) is sufficient in real implementation to reach the error tolerance. In Figure 11, contour plots are shown for a = 0.4 and b = 0.12 with various orientations of $\overline{\theta} = \pi/8$, $\overline{\theta} = \pi/4$ and $\overline{\theta} = 3\pi/8$, and it is anti-symmetric to the horizontal axis.

Case 2. *Two circular holes* [11,12]

Here, we consider a circular beam with two circular holes under bending as shown Fig. 12. One of the holes is concentric, and the other lies on the $x-axis$. In order to compare with the Bird and Steele's result, we assume R = 16 and b = 1, respectively, and all the numerical results are also obtained by using ten terms of Fourier series (M = 10). The stress concentration at the point P versus D/d (D is the distance between the two holes) is shown in Fig. 13. The stress concentration is expected to approach the case of a single hole in the center of beam when D/d becomes large. The contour of stress concentration for the case of D/d = 0.0625 is shown in Fig. 14, where d is the diameter of the hole. Our numerical results are well compared with the Bird and Steele's data.

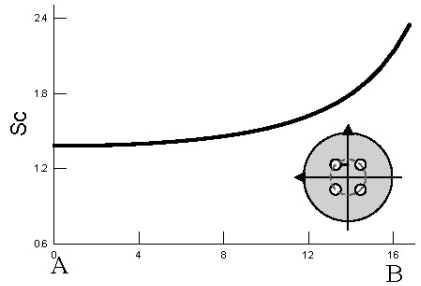

(a) *Sc* along *AB* (Present method)

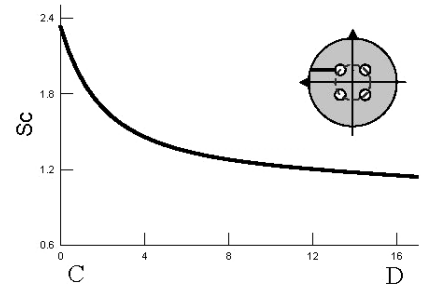

(b) *Sc* along *CD* (Present method)

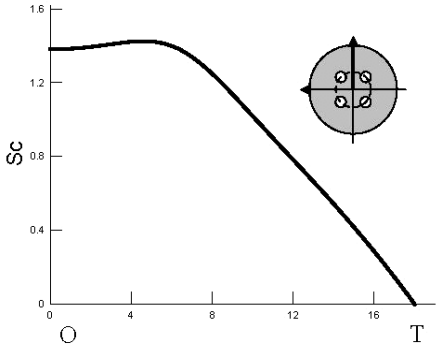

(c) *Sc* along *OT* (Present method)

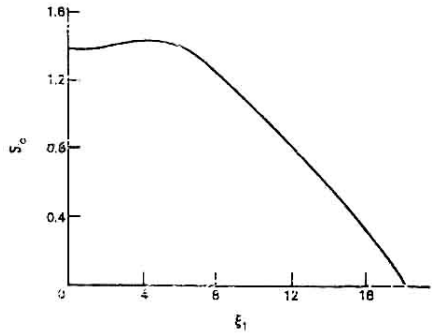

(d) *Sc* along *AB* (Naghdi's result) [11]

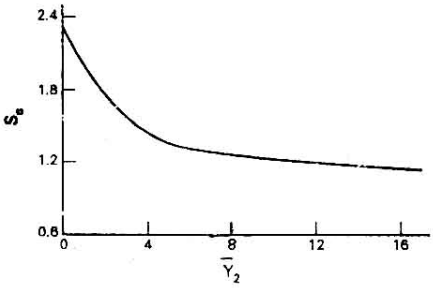

(e) *Sc* along *CD* (Naghdi's result)

Fig. 5 The stress concentration for a = 0.5, $\overline{\theta} = \pi/4$ and b = 0.1 [11]

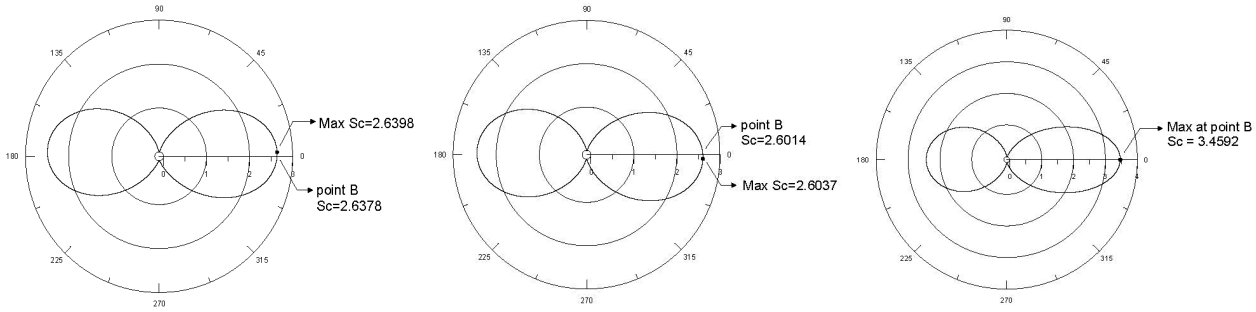

(a) $\bar{\theta} = 22.5$ (b) $\bar{\theta} = 45$ (c) $\bar{\theta} = 67.5$

Fig. 6 Stress concentrations around the third circle

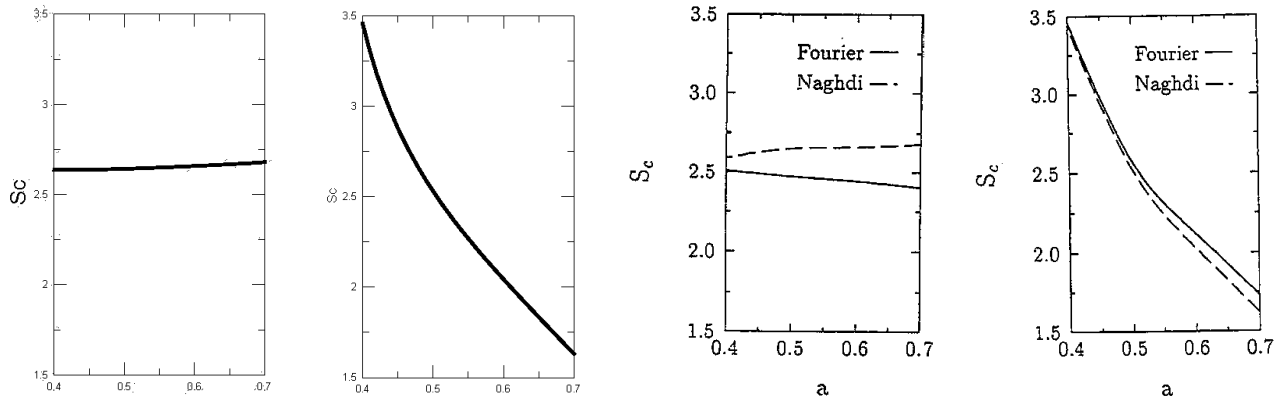

(a) $\bar{\theta} = \pi/8$ (Present method) (b) $\bar{\theta} = 3\pi/8$ (Present method) (c) $\bar{\theta} = \pi/8$ (Bird's result) [12] (d) $\bar{\theta} = 3\pi/8$ (Bird's result) [12]

Fig. 7 Stress concentration versus *a* for *b* = 0.12 of $\bar{\theta} = \pi/8$ and $\bar{\theta} = 3\pi/8$, respectively

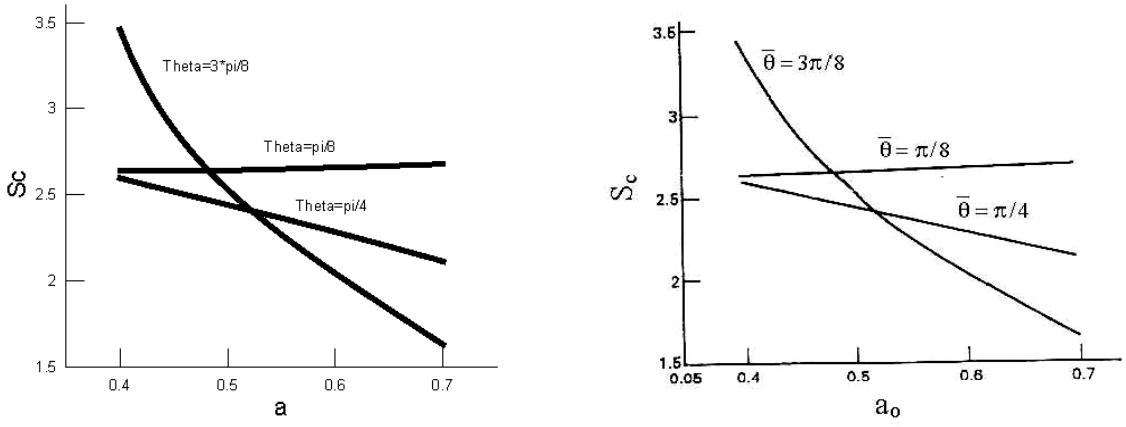

(a) Sc at point B (Present method) (b) Sc at point B (Naghdi's result) [11]

Fig. 8 Stress concentration versus *a* for *b* = 0.12 and three different values of $\bar{\theta} = \pi/8$, $\bar{\theta} = \pi/4$ and $\bar{\theta} = 3\pi/8$

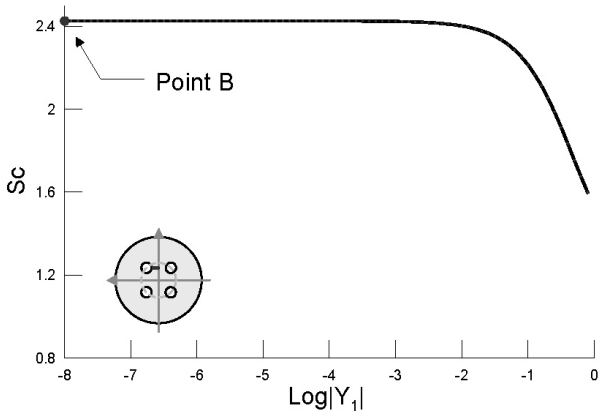

Fig. 9 Stress concentration along $\overline{AB}$ and extremely near point B for $a = 5$, $b = 1$, $R = 10$ and $\overline{\theta} = \pi/4$

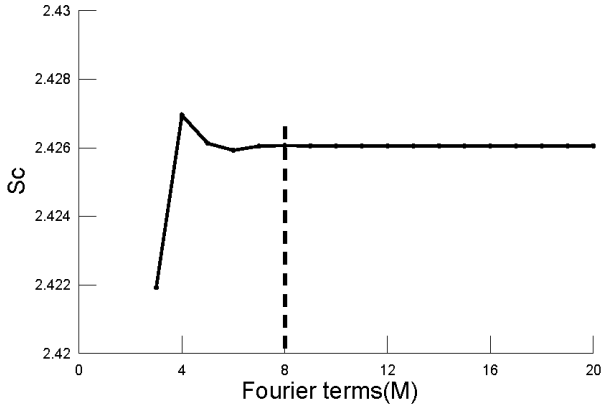

Fig. 10 Stress concentration on point B for $a = 0.5$, $\overline{\theta} = \pi/4$ and $b = 0.1$

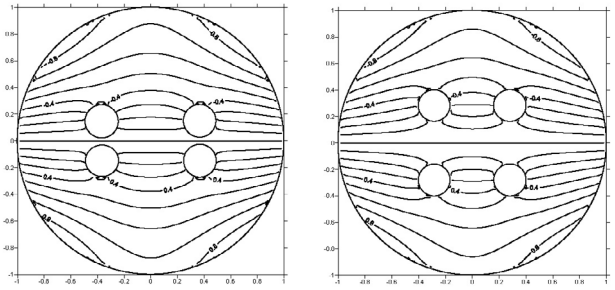

(a) $\overline{\theta} = \pi/8$ (b) $\overline{\theta} = \pi/4$

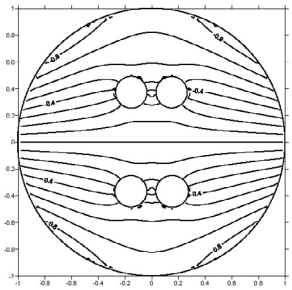

(c) $\overline{\theta} = 3\pi/8$

Fig. 11 Contour plots for $a = 0.4$, $b = 0.12$ and three different values of $\overline{\theta} = \pi/8$, $\overline{\theta} = \pi/4$ and $\overline{\theta} = 3\pi/8$

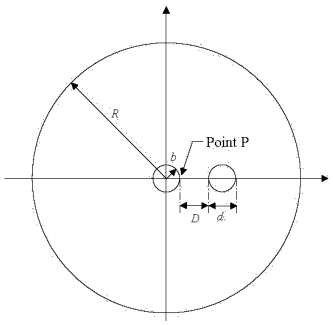

Fig. 12 Cantilever beam under bending weakened by two holes on $x-axis$

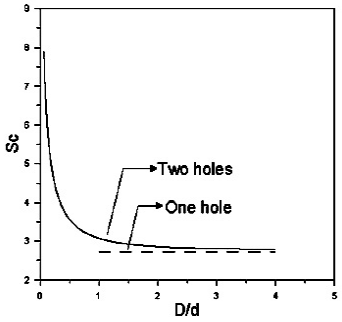

(a) Present method

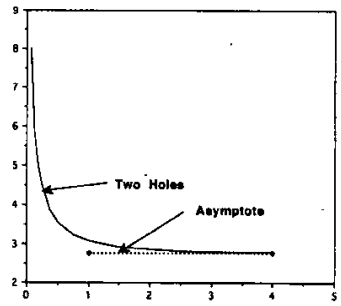

(b) Bird and Steele's result

Fig. 13 Stress concentration versus D/d of point P

8. CONCLUSIONS

For the bending problems with circular holes, we have proposed a BIEM formulation by using degenerate kernels, null-field integral equation and Fourier series in companion with adaptive observer systems and vector decomposition. This method is a semi-analytical approach since only truncation error in the Fourier series is involved. An advantage of the method over the Naghdi's [11] approach is that the extension to multiple circular holes of arbitrary radii and positions is straightforward. Results obtained by the present approach matched well with those of Naghdi's [11] although Bird and Steele's data [12] seems to deviate. The other gain of present method over BEM is free of boundary-layer effect. Although only two and four holes were tested to compare with the Naghdi [11] and Bird and Steele's [12] results, our general-purpose program can solve problems with arbitrary number and various positions of circular holes.

APPENDIX

Analytical evaluation of the integrals and their limits

	$U(\mathrm{s},\mathrm{x})$ and $\int_{\mathrm{B}} U(\mathrm{s},\mathrm{x})\,t(\mathrm{s})\,dB(\mathrm{s})$	$T(\mathrm{s},\mathrm{x})$ and $\int_{\mathrm{B}} T(\mathrm{s},\mathrm{x})\,u(\mathrm{s})\,dB(\mathrm{s})$
Degenerate kernel	$U(\mathrm{s},\mathrm{x}) = \begin{cases} U^i(R,\theta;\rho,\phi) = \ln R - \sum_{m=1}^{\infty} \frac{1}{m}\left(\frac{\rho}{R}\right)^m \cos\left(m(\theta-\phi)\right), & R \geq \rho \\ U^e(R,\theta;\rho,\phi) = \ln \rho - \sum_{m=1}^{\infty} \frac{1}{m}\left(\frac{R}{\rho}\right)^m \cos\left(m(\theta-\phi)\right), & R < \rho \end{cases}$	$T(\mathrm{s},\mathrm{x}) = \begin{cases} T^i(R,\theta;\rho,\phi) = \frac{1}{R} + \sum_{m=1}^{\infty} \frac{\rho^m}{R^{m+1}} \cos\left(m(\theta-\phi)\right), & R > \rho \\ T^e(R,\theta;\rho,\phi) = -\sum_{m=1}^{\infty} \frac{R^{m-1}}{\rho^m} \cos\left(m(\theta-\phi)\right), & R < \rho \end{cases}$
Orthogonal process	$\begin{cases} \int_0^{2\pi}\left[\ln R - \sum_{m=1}^{\infty} \frac{1}{m}\left(\frac{\rho}{R}\right)^m \cos\left(m(\theta-\phi)\right)\right]\cos(n\theta)\,Rd\theta = \pi\frac{1}{n}\frac{\rho^n}{R^{n-1}}\cos(n\phi), & R \geq \rho \\ \int_0^{2\pi}\left[\ln R - \sum_{m=1}^{\infty} \frac{1}{m}\left(\frac{\rho}{R}\right)^m \cos\left(m(\theta-\phi)\right)\right]\sin(n\theta)\,Rd\theta = \pi\frac{1}{n}\frac{\rho^n}{R^{n-1}}\sin(n\phi), & R \geq \rho \\ \int_0^{2\pi}\left[\ln \rho - \sum_{m=1}^{\infty} \frac{1}{m}\left(\frac{R}{\rho}\right)^m \cos\left(m(\theta-\phi)\right)\right]\cos(n\theta)\,Rd\theta = \pi\frac{1}{n}\frac{R^{n+1}}{\rho^n}\cos(n\phi), & R < \rho \\ \int_0^{2\pi}\left[\ln \rho - \sum_{m=1}^{\infty} \frac{1}{m}\left(\frac{R}{\rho}\right)^m \cos\left(m(\theta-\phi)\right)\right]\sin(n\theta)\,Rd\theta = \pi\frac{1}{n}\frac{R^{n+1}}{\rho^n}\sin(n\phi), & R < \rho \end{cases}$	$\begin{cases} \int_0^{2\pi}\left[\frac{1}{R} + \sum_{m=1}^{\infty} \frac{\rho^m}{R^{m+1}} \cos\left(m(\theta-\phi)\right)\right]\cos(n\theta)\,Rd\theta = \pi\left(\frac{\rho}{R}\right)^n \cos(n\phi), & R > \rho \\ \int_0^{2\pi}\left[\frac{1}{R} + \sum_{m=1}^{\infty} \frac{\rho^m}{R^{m+1}} \cos\left(m(\theta-\phi)\right)\right]\sin(n\theta)\,Rd\theta = \pi\left(\frac{\rho}{R}\right)^n \sin(n\phi), & R > \rho \\ \int_0^{2\pi}\left[-\sum_{m=1}^{\infty} \frac{R^{m-1}}{\rho^m} \cos\left(m(\theta-\phi)\right)\right]\cos(n\theta)\,Rd\theta = -\pi\left(\frac{R}{\rho}\right)^n \cos(n\phi), & R < \rho \\ \int_0^{2\pi}\left[-\sum_{m=1}^{\infty} \frac{R^{m-1}}{\rho^m} \cos\left(m(\theta-\phi)\right)\right]\sin(n\theta)\,Rd\theta = -\pi\left(\frac{R}{\rho}\right)^n \sin(n\phi), & R < \rho \end{cases}$
Limit $\rho \to R$	$\begin{cases} \pi\frac{1}{n}\frac{\rho^n}{R^{n-1}}\cos(n\phi) = \pi\frac{1}{n}R\cos(n\phi), & R \geq \rho \\ \pi\frac{1}{n}\frac{\rho^n}{R^{n-1}}\sin(n\phi) = \pi\frac{1}{n}R\sin(n\phi), & R \geq \rho \\ \pi\frac{1}{n}\frac{R^{n+1}}{\rho^n}\cos(n\phi) = \pi\frac{1}{n}R\cos(n\phi), & R < \rho \\ \pi\frac{1}{n}\frac{R^{n+1}}{\rho^n}\sin(n\phi) = \pi\frac{1}{n}R\sin(n\phi), & R < \rho \end{cases}$ (Continuous for $R^- < \rho < R^+$)	$\begin{cases} \pi\left(\frac{\rho}{R}\right)^n \cos(n\phi) = \pi\cos(n\phi), & R > \rho \\ \pi\left(\frac{\rho}{R}\right)^n \sin(n\phi) = \pi\sin(n\phi), & R > \rho \\ -\pi\left(\frac{R}{\rho}\right)^n \cos(n\phi) = -\pi\cos(n\phi), & R < \rho \\ -\pi\left(\frac{R}{\rho}\right)^n \sin(n\phi) = -\pi\sin(n\phi), & R < \rho \end{cases}$ (jump for $R^- < \rho < R^+$)
	$L(\mathrm{s},\mathrm{x})$ and $\int_{\mathrm{B}} L(\mathrm{s},\mathrm{x})\,t(\mathrm{s})\,dB(\mathrm{s})$	$M(\mathrm{s},\mathrm{x})$ and $\int_{\mathrm{B}} M(\mathrm{s},\mathrm{x})\,u(\mathrm{s})\,dB(\mathrm{s})$
Degenerate kernel	$L(\mathrm{s},\mathrm{x}) = \begin{cases} L^i(R,\theta;\rho,\phi) = -\sum_{m=1}^{\infty} \frac{\rho^{m-1}}{R^m} \cos\left(m(\theta-\phi)\right), & R > \rho \\ L^e(R,\theta;\rho,\phi) = \frac{1}{\rho} + \sum_{m=1}^{\infty} \frac{R^m}{\rho^{m+1}} \cos\left(m(\theta-\phi)\right), & R < \rho \end{cases}$	$M(\mathrm{s},\mathrm{x}) = \begin{cases} M^i(R,\theta;\rho,\phi) = \sum_{m=1}^{\infty} m\frac{\rho^{m-1}}{R^{m+1}} \cos\left(m(\theta-\phi)\right), & R \geq \rho \\ M^e(R,\theta;\rho,\phi) = \sum_{m=1}^{\infty} m\frac{R^{m-1}}{\rho^{m+1}} \cos\left(m(\theta-\phi)\right), & R < \rho \end{cases}$
Orthogonal process	$\begin{cases} \int_0^{2\pi}\left[-\sum_{m=1}^{\infty} \frac{\rho^{m-1}}{R^m} \cos\left(m(\theta-\phi)\right)\right]\cos(n\theta)\,Rd\theta = -\pi\left(\frac{\rho}{R}\right)^{n-1} \cos(n\theta), & R > \rho \\ \int_0^{2\pi}\left[-\sum_{m=1}^{\infty} \frac{\rho^{m-1}}{R^m} \cos\left(m(\theta-\phi)\right)\right]\sin(n\theta)\,Rd\theta = -\pi\left(\frac{\rho}{R}\right)^{n-1} \sin(n\theta), & R > \rho \\ \int_0^{2\pi}\left[\frac{1}{\rho} + \sum_{m=1}^{\infty} \frac{R^m}{\rho^{m+1}} \cos\left(m(\theta-\phi)\right)\right]\cos(n\theta)\,Rd\theta = \pi\left(\frac{R}{\rho}\right)^{n+1} \cos(n\theta), & R < \rho \\ \int_0^{2\pi}\left[\frac{1}{\rho} + \sum_{m=1}^{\infty} \frac{R^m}{\rho^{m+1}} \cos\left(m(\theta-\phi)\right)\right]\sin(n\theta)\,Rd\theta = \pi\left(\frac{R}{\rho}\right)^{n+1} \sin(n\theta), & R < \rho \end{cases}$	$\begin{cases} \int_0^{2\pi}\left[\sum_{m=1}^{\infty} m\frac{\rho^{m-1}}{R^{m+1}} \cos\left(m(\theta-\phi)\right)\right]\cos(n\theta)\,Rd\theta = n\pi\frac{\rho^{n-1}}{R^n}\cos(n\theta), & R \geq \rho \\ \int_0^{2\pi}\left[\sum_{m=1}^{\infty} m\frac{\rho^{m-1}}{R^{m+1}} \cos\left(m(\theta-\phi)\right)\right]\sin(n\theta)\,Rd\theta = n\pi\frac{\rho^{n-1}}{R^n}\sin(n\theta), & R \geq \rho \\ \int_0^{2\pi}\left[\sum_{m=1}^{\infty} m\frac{R^{m-1}}{\rho^{m+1}} \cos\left(m(\theta-\phi)\right)\right]\cos(n\theta)\,Rd\theta = n\pi\frac{R^n}{\rho^{n+1}}\cos(n\theta), & R < \rho \\ \int_0^{2\pi}\left[\sum_{m=1}^{\infty} m\frac{R^{m-1}}{\rho^{m+1}} \cos\left(m(\theta-\phi)\right)\right]\sin(n\theta)\,Rd\theta = n\pi\frac{R^n}{\rho^{n+1}}\sin(n\theta), & R < \rho \end{cases}$
Limit $\rho \to R$	$\begin{cases} -\pi\left(\frac{\rho}{R}\right)^{n-1} \cos(n\phi) = -\pi\cos(n\phi), & R > \rho \\ -\pi\left(\frac{\rho}{R}\right)^{n-1} \sin(n\phi) = -\pi\sin(n\phi), & R > \rho \\ \pi\left(\frac{R}{\rho}\right)^{n+1} \cos(n\phi) = \pi\cos(n\phi), & R < \rho \\ \pi\left(\frac{R}{\rho}\right)^{n+1} \sin(n\phi) = \pi\sin(n\phi), & R < \rho \end{cases}$ (jump for $R^- < \rho < R^+$)	$\begin{cases} n\pi\frac{\rho^{n-1}}{R^n}\cos(n\phi) = n\pi\frac{1}{R}\cos(n\phi), & R \geq \rho \\ n\pi\frac{\rho^{n-1}}{R^n}\sin(n\phi) = n\pi\frac{1}{R}\sin(n\phi), & R \geq \rho \\ n\pi\frac{R^n}{\rho^{n+1}}\cos(n\phi) = n\pi\frac{1}{R}\cos(n\phi), & R < \rho \\ n\pi\frac{R^n}{\rho^{n+1}}\sin(n\phi) = n\pi\frac{1}{R}\cos(n\phi), & R < \rho \end{cases}$ (Continuous for $R^- < \rho < R^+$)

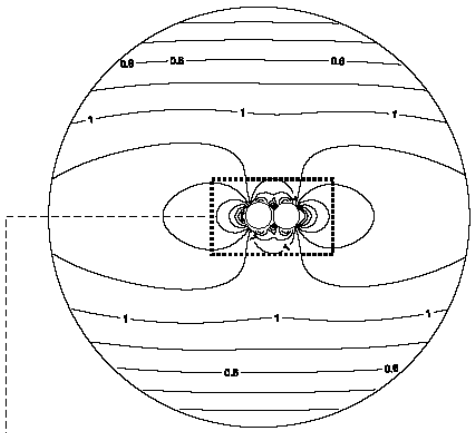

(a) Present result

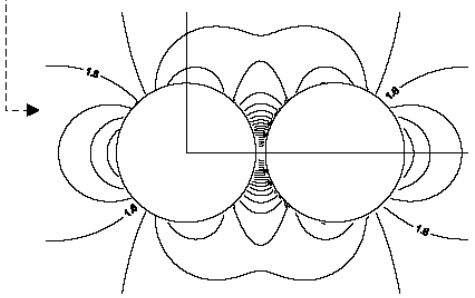

(b) Present result (local)

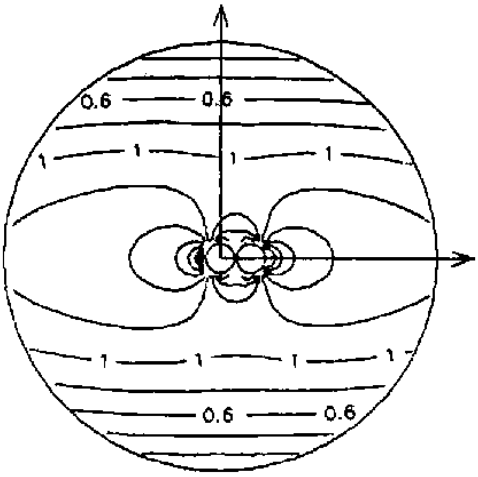

(c) Bird and Steele's result [12]

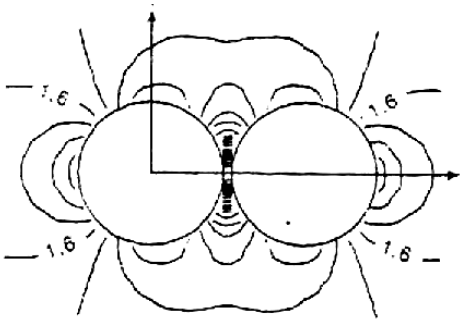

(d) Bird and Steele's result (local) [12]

Fig. 14 Contour of stress concentration of $D/d = 0.0625$

ACKNOWLEDGEMENTS

The study is supported by the National Science Council of Taiwan, the Republic of China through the grant number NSC 94-2211-E-019-009.

REFERENCES

1. Hwu, C. B., "Stroh Formalism and its Extensions to Coupled Inplane-bending Problems," *The Chinese Journal of Mechanics — Series A*, 19, pp. 41–53 (2003).
2. Shiah, Y. C., Fang, J., Wei, C. Y. and Liang, Y. C., "In-plane Bending Fracture of a Large Beam Containing a Circular-arc Crack," *The Chinese Journal of Mechanics —Series A*, 18, pp. 145–151 (2002).
3. Huang, C. S., "Analysis of Stress Singularities at Bi-material Corners in Reddy's Theory of Plate Bending," *Journal of Mechanics*, 22, pp. 67–75 (2006).
4. Sokolnikoff, I. S., *Mathematical Theory of Elasticity, McGraw-Hill*, New York (1956).
5. Timoshenko, S. P. and Goodier, J. N., *Theory of Elasticity*, McGraw-Hill, New York (1970).
6. Chou, S. I., "Stress Field around Holes in Antiplane Shear Using Complex Variable Boundary Element Method," *ASME J. Applied Mechanics*, 64, pp. 432–435 (1997).
7. Ang, W. T. and Kang, I., "A Complex Variable Boundary Element Method for Elliptic Partial Differential Equations in a Multiply-connected Region," *Int. J. Computer Mathematics*, 75, pp. 515–525 (2000).
8. Hromadka, T. V. and Lai, C., *The Complex Variable Boundary Element Method in Engineering Analysis*, Springer-Verlag, New York (1986).
9. Honein, E., Honein, T. and Herrmann, G., "Further Aspects of the Elastic Field for Two Circular Inclusions in Antiplane Elastostatics," *ASME J. Applied Mechanics*, 59, pp. 774–779 (1992).
10. Chen, J. T., Shen, W. C. and Wu, A. C., "Null-field Integral Equations for Stress Field around Circular Holes under Anti-plane Shear," *Engineering Analysis with Boundary Elements*, 30, pp. 205–217 (2006).
11. Naghdi, A. K., "Bending of a Perforated Circular Cylindrical Cantilever," *Int. J. Solids and Structures*, 28, pp. 739–749 (1991).
12. Bird, M. D. and Steele, C. R., "A Solution Procedure for Laplace's Equation on Multiply Connected Circular Domains," *ASME J. Applied Mechanics*, 59, pp. 398–404 (1992).
13. Chen, J. T. and Hong, H.-K., "Review of Dual Boundary Element Methods with Emphasis on Hypersingular Integrals and Divergent Series," *Applied Mechanics Reviews, ASME*, 52, pp. 17–33 (1999).
14. Chen, J. T. and Chiu, Y. P., "On the Pseudo-differential Operators in the Dual Boundary Integral Equations Using Degenerate Kernels and Circulants," *Engineering Analysis with Boundary Elements*, 26, pp. 41–53 (2002).

15. Chen, J. T., Lin, J. H., Kuo, S. R. and Chiu, Y. P., "Analytical Study and Numerical Experiments for Degenerate Scale Problems in Boundary Element Method Using Degenerate Kernels and Circulants," *Engineering Analysis with Boundary Elements*, 25, pp. 819–828 (2001).
16. Chen, J. T., Lee, C. F., Chen, I. L. and Lin, J. H., "An Alternative Method for Degenerate Scale Problem in Boundary Element Methods for the Two-dimensional Laplace Equation," *Engineering Analysis with Boundary Elements*, 26, pp. 559–569 (2002).
17. Chen, J. T., Kuo, S. R. and Lin, J. H., "Analytical Study and Numerical Experiments for Degenerate Scale Problems in the Boundary Element Method for Two-Dimensional Elasticity," *Int. J. Numerical Methods in Engineering*, 54, pp. 1669–1681 (2002).
18. Bird, M. D. and Steele, C. R., "A Solution Procedure for Laplace's Equation on Multiply Connected Circular Domains," *ASME J. Applied Mechanics*, 59, pp. 398–404 (1992).

(Manuscript received June 13, 2006,
accepted for publication August 24, 2006.)